Biogeosciences Discuss., 11, 8713–8748, 2014
www.biogeosciences-discuss.net/11/8713/2014/
doi:10.5194/bgd-11-8713-2014
© Author(s) 2014. CC Attribution 3.0 License.

Biogeosciences Discussions
Open Access

This discussion paper is/has been under review for the journal Biogeosciences (BG).
Please refer to the corresponding final paper in BG if available.

Spatio-temporal variations of nitrogen isotopic records in the Arabian Sea

S.-J. Kao[1], B. Wang[1], L. Zheng[1], K. Selvaraj[1], S.-C. Hsu[2], X. Wan[1], M. Xu[1], and C.-T. A. Chen[3]

[1]State Key Laboratory of Marine Environmental Science, Xiamen University, Xiamen, China
[2]Research Center for Environmental Changes, Academia Sinica, Taipei, Taiwan
[3]Institute of Marine Geology and Chemistry, National Sun Yat-sen University, Kaohsiung, Taiwan

Received: 3 May 2014 – Accepted: 26 May 2014 – Published: 11 June 2014

Correspondence to: S.-J. Kao (sjkao@xmu.edu.cn)

Published by Copernicus Publications on behalf of the European Geosciences Union.

Abstract

Nitrogen and carbon contents vs. their isotopic compositions for past 35 ka for a sediment core (SK177/11) collected from the most southeastern part of the Arabian Sea (AS) were presented. A one-step increase in $\delta^{15}N_{bulk}$ starting at the deglaciation with a corresponding decrease in $\delta^{13}C_{TOC}$ was found similar to documentation elsewhere which showed a global coherence in general. We synthesized available reports including dissolved oxygen, $\delta^{15}N$ of nitrate ($\delta^{15}N_{NO_3}$), as well as $\delta^{15}N$ of total nitrogen ($\delta^{15}N_{bulk}$) for trap material and surface/downcore sediments in the AS in order to explore the past nitrogen dynamics in the Arabian Sea. According to 25 µmol kg^{-1} dissolved oxygen isopleth at 150 m deep, we classified all reported data into northern and southern groups. We obtained geographically distinctive bottom-depth effects for northern and southern AS at different climate stages. By eliminating the bias caused by bottom depth, the modern day sedimentary $\delta^{15}N_{bulk}$ values largely reflect the $\delta^{15}N_{NO_3}$ supply from the bottom of the euphotic zone; meanwhile, the diffusive sedimentary $\delta^{15}N_{bulk}$ in long cores became confined revealing a more consistent pattern except recent 6 ka. The nitrogen cycle in entire AS apparently responded to open-ocean changes until 6 ka, during which further enhanced denitrification in the northern AS was likely local and driven by monsoon; while in the southern AS either nitrogen fixation was enhanced correspondingly to the continuously reduced $\delta^{15}N_{bulk}$ for a compensation or the decreasing trend just followed the global pattern dominated by a longer term coupling of N_2 fixation and denitrification.

1 Introduction

Nitrogen biogeochemical processes in the ocean are intimately related to various elemental cycles synergistically modulate atmospheric CO_2 and N_2O concentrations, thus feedback to climate in millennium scale (Gruber, 2004; Falkowski and Godfrey, 2008; Altabet et al., 2002). Oxygen deficient zones (ODZs) though occupies only ~4 % of

BGD
11, 8713–8748, 2014

ocean volume the denitrification process therein contributes remarkably to the losses of nitrate leaving excess P in the remaining water mass to stimulate N_2-fixation while entering euphotic zone (Morrison et al., 1998; Deutsch et al., 2007) thus control the budget of bio-available nitrogen in ocean. Denitrification leaves $^{15}NO_3^-$ in residual nitrate (Sigman et al., 2001), by contrast, N_2-fixation introduces new bio-available nitrogen with low $\delta^{15}N$ values (Capone et al., 1997) into ocean for compensation. The Arabian Sea (AS), as one of the three largest ODZs in the world with distinctive monsoon driven upwelling, accounts for at least one third of the loss of marine fixed Nitrogen (Codispoti and Christensen, 1985) playing an important role in the past climate via regulating atmospheric N_2O concentration (Agnihotri et al., 2006) or nitrogen inventory which further modulates CO_2 sequestration by biological pump (Altabet, 2006).

Sedimentary nitrogen isotope, measured as standard δ notation with respect to standards of atmospheric nitrogen, is an important tool to study past marine nitrogen cycle. Nitrogen isotope compositions of sedimentary organic matter potentially reflect biological processes in water column, such as denitrification (Altabet et al., 1995; Ganeshram et al., 1995, 2000), nitrogen fixation (Haug et al., 1998), and the degree of nitrate utilization by algae (Altabet and Francois, 1994; Holmes et al., 1996; Robinson et al., 2004). However, alteration may occur before the signal of $\delta^{15}N$ of exported production is buried. Altabet and Francois (1994) reported little diagenetic alteration of the near-surface $\delta^{15}N$ in the equatorial Pacific, while an apparent +5 ‰ diagenetic enrichment relative to sinking particles in the southern ocean south of the polar front. In the Sargasso Sea, sedimentary $\delta^{15}N$ also enriched by $3 \sim 6$ ‰ relative to sinking particles (Altabet et al., 2002; Gruber and Galloway, 2008). The degree of alteration was attributed to particle sinking rate and OM preservation (Altabet, 1988). Gaye-Haake et al. (2005) also suggested that low sedimentation rates benefit organic matter decomposition resulting in positive shift in bulk sedimentary $\delta^{15}N$ comparing to sinking particles in South China Sea. Finally, Robinson et al. (2012) concluded that oxygen exposure time at the seafloor is the dominant factor controlling the extent of N isotopic alteration.

BGD
11, 8713–8748, 2014

Previous measurements of $\delta^{15}N_{bulk}$ in various cores and surface sediments in the AS showed: (1) near-surface NO_3^- in AS is completely utilized in an annual cycle, resulting in small isotopic fractionation between $\delta^{15}N$ of exported sinking particles and $\delta^{15}N$ of NO_3^- supplied to the euphotic zone (Altabet, 1988; Thunell et al., 2004); (2) monsoon-driven surface productivity and associated oxidant demand are regarded as the main control on water column denitrification in the past (Ganeshram et al., 2000; Ivanochko et al., 2005); (3) sedimentary $\delta^{15}N_{bulk}$ primarily reflects the relative intensity of water column denitrification in this area (Altabet et al., 1995, 1999); (4) oxygen supply at intermediate depth by the Antarctic Intermediate Waters (AAIW) can modulate the denitrification intensity in northern AS (Schulte et al., 1999; Schmittner et al., 2007; Pichevin et al., 2007). Among previous researches, the geographic features in sedimentary $\delta^{15}N_{bulk}$ between north and south basins has yet been discussed, particularly, on the basis of bottom-depth effect which might be different during glacial and interglacial periods.

In this study, a sediment core (SK177/11) collected from the slope of southeastern AS was measured for organic C and N contents, stable C and N isotopes. We also synthesize documented hydrography and isotope data, such as dissolved oxygen (DO), N* ($N^* = NO_3^- - 16 \times PO_4^{3-} + 2.9$, Gruber and Sarmiento, 2002), and $\delta^{15}N$ of nitrate, trapped material and surface/downcore sediments, among which surface and downcore sediments experienced more intensified diagenetic alteration. In this study, we separate Arabian Sea into north and south basins according to subsurface DO of 25 µmol kg^{-1} isopleths at 150 m and classify sediments by time span (glacial, Holocene and modern) for comparison. We aim to (1) investigate the geographic and glacial-interglacial differences in bottom-depth effect and to (2) retrieve extra information from sedimentary $\delta^{15}N_{bulk}$ by removing basin/climate stage specific bottom-depth effects, thus, better decipher the environmental history of the Arabian Sea.

BGD
11, 8713–8748, 2014

2 Study area

The Arabian Sea is characterized by seasonal reversal of monsoon winds, resulting in large seasonal physical/hydrographic/biological/chemical variations in water column (Nair et al., 1989). Cold and dry northeasterly winds blow during winter from high-pressure cell of the Tibetan Plateau, whereas heating of the Tibetan Plateau in summer (June to September) reverses the pressure gradient leading to warm and moist south-westerly winds and precipitation maximum. In present day, the SW monsoon is much stronger than its northeastern counterpart. Consistent seasonal oscillation in surface biological productivity was also revealed by satellite pictures in the entire Arabian Sea.

The spatial distribution of DO at 150 m deep for the AS is shown in Fig. 1a (World Ocean Atlas 2009, http://www.nodc.noaa.gov/OC5/WOA09/woa09data.html), which shows a clear southward increasing pattern with DO increased from ~ 5 to $> 100\,\mu mol\,kg^{-1}$ and the lowest DO value appears at the northeast of the northern basin. As denitrification, the dominant nitrate removal process, generally occurs in the water column where DO concentration ranges $0.7 \sim 20\,\mu mol\,kg^{-1}$ (Paulmier et al., 2009), the intensity of denitrification was reported to descend gradually, corresponding with the DO spatial pattern from northern to southern of AS, and became unobvious at 11 or 12° N (Naqvi et al., 1982). As indicated by upper 2000 m N–S transect of DO (Fig. 1b) a southward decreasing in OMZ thickness can be observed and the contour line of $5\,\mu mol\,kg^{-1}$ extends to around 13° N. Since the nitrate source is mainly from the bottom of euphotic zone at around 150 m we postulate a geographically distinctive sedimentary $\delta^{15}N_{bulk}$ underneath OMZ. Thus, an isopleths of $25\,\mu mol\,kg^{-1}$ DO at 150 m is applied as a geographic boundary to separate the northern and southern part of AS basin. The interface where DO concentration changed from 20 to $30\,\mu mol\,kg^{-1}$ was such a transition zone. On the other hand, the bottom layer of OMZ moves shallower toward south and a similar longitudinal pattern of bottom DO with high values at the southern basin had been shown previously (Gouretski and Koltermann, 2004).

BGD
11, 8713–8748, 2014

Accordingly, the bottom oxygen content may also be a factor to influence the degree of alteration in sedimentary $\delta^{15}N_{bulk}$.

As mentioned in Introduction, nitrate is removed via denitrification in ODZs resulting in excess P to stimulate N_2-fixation. Figure 1c shows the N–S transect of N*, which represents nitrate deficit (Gruber and Darmieto, 2002), for the upper 2000 m. Overall, the entire water column is negative in N* (P-excess) and the lowest N* value appears at ~ 300 m at 19–20° N, where DO is <1 µmol kg^{-1}. Meanwhile, a gradually southward increase in N* can be observed for upper 100 m and the isopleth of N* of −4 deepens southward with the highest N* (−3) appearing at ~ 10–12° N. The vertical expansion of high N* water column as well as a simultaneous increase in N* strongly indicate an addition of bio-available nitrogen had occurred when surface water traveling southward.

3 Material and method

A sediment gravity core, SK-177/11 (8.2° N and 76.47° E), was collected at water depths of 776 m on the continental slope off southwest coast of India (Kerala) during the 177th cruise of ORV *SagarKanya* on October 2002. This is so far the reported sediment core locates at the most southern part of the AS. The 3.65 m long core was sub-sampled at intervals of 2 cm from top to 100 cm, and 5 cm from 100 cm to the bottom of the core (open circles in Fig. 2a). At 1.70 m we see an obvious boundary, above which sediments possessed by brownish grey clayey and greenish black clayey sediments occupied the lower part. Neither distinct laminations nor turbidities can be observed by visual contact immediately after collection or at the time during sub-sampling (Pandarinath et al., 2007). All sub-samples were freeze-dried and ground into powder in agate mortar. Sand was absent (< 1 wt%) throughout the core.

The calendar chronology for core SK177/11 was based on 7 accelerator mass spectrometry (AMS) radiocarbon (^{14}C) dates of bulk organic matter (Fig. 2a). Calendar years were calculated using calibration CALIB 6.0 with a reservoir age correction of 402 years (Stuiver et al., 1998; Reimer et al., 2009). Details on the ^{14}C age controlling

BGD
11, 8713–8748, 2014

points were presented in Table 1. Given that the AMS ^{14}C dates were obtained on organic matter samples, we may not be able to avoid the organics aging during transport (Mollenhauer et al., 2005) or interference by pre-aged organics sourced from land (Kao et al., 2008). However, besides the reservoir age correction, the organic matters were in high contents (TOC range 2.2 ~ 5.5 %) and mostly consisted of marine originated compounds (as confirmed by stable C isotope data and C/N ratio shown in Figs. 3b and 4).

Bulk sedimentary nitrogen content and $\delta^{15}N$ analyses were carried out using a Carlo-Erba EA 2100 elemental analyzer connected to a Thermo Finnigan Delta V Advantage isotope ratio mass spectrometer (EA-IRMS). Sediments for total organic carbon (TOC) analyses were acid-treated with 1N HCl for 16 h, and then centrifuged to remove carbonate. The acid-treated sediments were further dried at 60 °C for TOC content and $\delta^{13}C$. The nitrogen isotopic compositions of acidified samples were obtained in the same time for comparison. Carbon and nitrogen isotopic data were presented by standard δ notation with respect to PDB carbon and atmospheric nitrogen. USGS 40, which has certified $\delta^{13}C$ of −26.24 ‰ and $\delta^{15}N$ of −4.52 ‰ and acetanilide (Merck) with $\delta^{13}C$ of −29.76 ‰ and $\delta^{15}N$ of −1.52 ‰ were used as working standards. The reproducibility of carbon and nitrogen isotopic measurements is better than 0.15 ‰. The precision of nitrogen and carbon content measurements were better than 0.02 % and 0.05 %, respectively. Meanwhile, the acidified and non-acidified samples exhibited identical patterns in $\delta^{15}N$ (not shown) with mean deviation of 0.3 ‰.

4 Results

4.1 Sedimentation rate

The age-depth curve was shown in Fig. 2a, in which age dates were evenly distributed throughout the core though not high resolution. In Mullenhauer et al. (2005), the largest age offset between total organic carbon and co-occurring foraminifera is ~ 3000 years

BGD
11, 8713–8748, 2014

and mostly < 2000 years. Meanwhile, the offset remains more or less constant throughout past 20 ka regardless of the deglacial transition. The youngest date in our core is 3180 cal ka BP at 58 cm. We may expect younger age on the surface. Thus, if our TOC samples contain any pre-aged organics as indicated by Mullenhaure et al. (2005), the offset should not be too large to alter our interpretation for the comparison between glacial and Holocene periods. The linear sedimentation rates derived from 5 date intervals range from 6 to 20 cm ka^{-1} (Fig. 2b), with relatively constant value (~ 6 cm ka^{-1}) prior to Holocene except the excursion around the last glacial maximum. The linear sedimentation rates started to increase since Holocene and reached 18 ~ 20 cm ka^{-1} when the sea level reached modern day level.

4.2 Nitrogen and carbon contents and their isotopes

Values of $\delta^{15}N_{bulk}$ ranged from 4.7‰ to 7.1‰ with significantly lower values during glacial period (Fig. 3a). The $\delta^{15}N$ values increased rapidly since ~ 19 ka BP, with a peak at ~ 15 ka BP and then started to decrease gradually toward modern day except the low $\delta^{15}N$ excursion at ~ 13 ka BP during the Younger-Dryas event. Figure 3b shows that values of $\delta^{13}C_{TOC}$ (−21.5 ~ −18.5‰) were consistent with the $\delta^{13}C$ of typical marine organic matter end-member (−22 ~ −18‰). An abrupt decrease in $\delta^{13}C$ was observed in concert with the dramatic decrease in $\delta^{15}N_{bulk}$ at the start of deglaciation.

Bulk nitrogen content (TN) had a range of 0.23 ~ 0.75 % (Fig. 3c) and the total organic carbon (TOC) content ranged from 2 % to 6 % (Fig. 3d). Both TN and TOC showed similar trend over the last 35 ka BP with relatively constant values prior to Holocene and an afterward elevation till modern day. Figure 4 shows the scatter plot of TOC against TN. The slope of the linear regression line for TOC against TN (TOC = (6.67 ± 0.22) × TN + (0.99 ± 0.11), $R^2 = 0.94$, $n = 57$, $p < 0.0001$) is 6.67 again indicating that organic matter is mainly marine-sourced. Though this slope is slightly higher than the Redfield ratio of 5.68 (wt./wt.), it is lower than that observed on the

BGD
11, 8713–8748, 2014

East China Sea shelf (7.46; Kao et al., 2003). Meanwhile, the intercept of TN is negative when TOC downs to zero implying that inorganic nitrogen can be ignored in our core (Schubert et al., 2001). Obviously, if we force the regression through the origin point, TOC/TN values for samples during the Holocene will have the lower ratios reflecting even less contribution from terrestrial organics.

5 Discussion

5.1 Downward transfer and transformation of N isotopic signal

The reported depth profiles of $\delta^{15}N_{NO_3}$ were shown in Fig. 5, in which $\delta^{15}N_{NO_3}$ values of water depth deeper than 1200 m range narrowly around 6 ~ 7 ‰, which is slightly higher than the global average of the deep oceans (4.8 ± 0.2 ‰ for > 2500 m, Sigman et al., 2000; 5.7 ± 0.7 for > 1500 m, Liu and Kaplan, 1989). Below the euphotic layer, $\delta^{15}N_{NO_3}$ increases rapidly peaking at around 200 ~ 400 m. The preferential removal of $^{14}NO_3$ by water column denitrification accounts for these subsurface $\delta^{15}N_{NO_3}$ highs (Brandes et al., 1998; Altabet et al., 1999; Naqvi et al., 2006). The subsurface $\delta^{15}N_{NO_3}$ maximum ranges from 10 to 18 ‰ for different stations implying a great spatial heterogeneity in water column denitrification intensity, noteworthy, in general the higher values appear in the northeastern AS (15 ~ 18 ‰) highlighting that focal area of water column denitrification is prone to northeastern Arabian Sea (Naqvi et al., 1994; Pichevin et al., 2007) as revealed by DO spatial distribution in Fig. 1a. Opposite to higher denitrification in the northeastern AS, the export production is always higher in the northwestern AS throughout a year (Rixen et al., 1996). Such decoupling between productivity and denitrification was attributed to the oxygen supply by intermediate water exchange besides primary productivity oxygen demand (Pichevin et al., 2007). Note that, the $\delta^{15}N_{NO_3}$ values at water depth of 100 ~ 150 m, which corresponds to the bottom depth of euphotic zone (Olson et al., 1993), from different stations fall within a narrow range of 7 ~ 9 ‰ despite of wide denitrification intensity underneath. The rapid addition of new

BGD
11, 8713–8748, 2014

nitrogen as mentioned earlier might account for the relatively uniform $\delta^{15}N_{NO_3}$ at the bottom of euphotic layer. Unfortunately, none $\delta^{15}N_{NO_3}$ profiles and sediment trap data are available for the southern basin for comparison.

Interestingly, reported $\delta^{15}N$ of sinking particles ($\delta^{15}N_{SP}$) collected by five sedimentation traps deployed from 500 m throughout 3200 m deep ranged narrowly within 5.1 ~ 8.5 ‰ (Fig. 6), which is slightly lower but overlaps largely with $\delta^{15}N_{NO_3}$ values at 100 ~ 150 m. Such similarity in $\delta^{15}N_{NO_3}$ at 100 ~ 150 m and sinking particles strongly indicated that (1) NO_3^- source for sinking particles was coming from the depth around 100 ~ 150 m instead of 200 ~ 400 m, the oxygen deficient zones (ODZs) where maximum $\delta^{15}N_{NO_3}$ value occurred (Schäfer and Ittekkot, 1993; Altabet et al., 1999) and (2) little alteration had occurred in $\delta^{15}N_{SP}$ along sinking in the water column as indicated by Altabet (2006). The five trap stations were the only available dataset in the AS (Gaye-Haaake et al., 2005). The trap locations were in the same area but little south comparing with $\delta^{15}N_{NO_3}$ stations (insert map in Fig. 6). The slightly lower $\delta^{15}N$ in sinking particle is attributable to their geographic locations (see below) since incomplete relative utilization of surface nitrate has been documented to have a very limited imprint on the $\delta^{15}N$ signal in the AS (e.g., Schäfer and Ittekkot, 1993).

The uniformly low values of $\delta^{15}N_{NO_3}$ at the bottom of euphotic zone should be a consequence resulted from various processes, such as remineralizaiton, nitrification and N_2-fixation, in the euphotic zone. Nevertheless, the distribution pattern of N* illustrates that there must be an addition of $^{14}NO_3$ into the system to cancelling out the isotopic enrichment caused by denitrification. Note that the positive offset in $\delta^{15}N_{NO_3}$ ($\Delta\delta^{15}N_{NO_3}$, 6 ~ 12 ‰) in ODZs caused by various degree of denitrification were narrowed down significantly while nitrate transports upward. This implies that the degree of addition processes, most likely the N_2-fixation, varied in concert with the intensity of denitrification underneath. The spatial coupling of denitrification and N_2-fixation by Deutsch et al. (2007) is supportive of this notion. Moreover, fixed N had been proved to ac-

BGD
11, 8713–8748, 2014

count for a significant part of surface nitrate in modern day AS where denitrification is exceptionally intense (Brandes et al., 1998; Capone et al., 1998; Parab et al., 2012).

Comparing with reported $\delta^{15}N$ of surface sediments retrieved from trap locations, a significant positive shift in $\delta^{15}N$ can be seen at the seafloor (Fig. 6). Such positive deviation can be seen elsewhere in previous reports (Altabet, 1988; Brummer et al., 2002; Kienast et al., 2005) due to prolonged oxygen exposure after deposition (Robinsson et al., 2012) associated with sedimentation rate (Pichevin et al., 2007). Although Cowie et al. (2009) found ambiguous relation between contents of sedimentary organic carbon and oxygen in deep water. They also noticed that the maximum of organic carbon contents appeared at the lower boundary of the OMZ, where oxygen contents were relatively enriched. Accordingly, they believed that there existed other factors controlling the preservation of organic carbon, such as the character of organic matters, the interaction between organic matters and minerals, the enrichment and activity of benthic organism, or the physical factor including the screening and water dynamic effect. In next section, we focus on $\delta^{15}N_{bulk}$ instead of the content of organic matter, according to our analysis we believed that DO concentration should be a major factor determining the degree of alteration in sedimentary $\delta^{15}N_{bulk}$.

5.2 Geographically-distinctive bottom depth effects in modern day

As classified by oxygen content of 25 µmol kg^{-1} at 150 m, documented surface sedimentary $\delta^{15}N_{bulk}$ (Gaye-Haake et al., 2005) were separated into northern and southern groups to examine the geographic difference in bottom effect. Both groups exhibit positive linear relationships between $\delta^{15}N_{bulk}$ and bottom depth (deeper than 200 m) (Fig. 7a). The regression equations were shown in Table 2. Interestingly, the regression differs statistically from each other in general in term of slope and intercept. The slope represents the degree of positive shift of sedimentary $\delta^{15}N$ due to bottom-depth effect. For the southern AS, the slope is $0.76\,(\pm 0.14) \times 10^{-3}$ km^{-1}, which is close to the correction factor (0.75×10^{-3} km^{-1}) for the world ocean proposed by Robinson et al. (2012) and further applied by Galbraith et al. (2012). By contrast, the slope for

BGD
11, 8713–8748, 2014

the northern AS is 0.55 (± 0.08) × 10^{-3} km^{-1}, which is significantly lower, implying that depth-associated alteration in northern AS is smaller. The correction factor for bottom-depth effect was suggested to vary in different regions such as that in the South China Sea (Gaye et al., 2009). Since the magnitude of oxygen exposure is the primary control of depth effect (Gaye-Haake et al., 2005; Mobius et al., 2011; Robinson et al., 2012), we attributed this lower slope in the northern AS to relatively higher sedimentation rates (not shown) and lower oxygen contents as indicated by previous researches (Olson et al., 1993; Morrison et al., 1999; Brummer et al., 2002).

On the other hand, the intercept for the northern AS regression is (8.1 ± 0.2), which is again significantly higher than that for the southern AS (6.0 ± 0.3). As aforementioned, $\delta^{15}N$ values of sinking particle resembled the $\delta^{15}N$ of nitrate sourced from 100 ~ 150 m deep; according to the depth-dependent correction factor we may convert sedimentary $\delta^{15}N_{bulk}$ values at various water depths into its initial condition when the digenetic alteration is minimal to represent the $\delta^{15}N$ of source nitrate. Higher intercept suggests a stronger denitrification had occurred in northern AS surface sediments. The 2.1 ‰ lower intercept in the southern AS likely reflects the addition of N_2-fixation in the upper water column while it travels southward. The progressive increase of N* toward southern AS supports our speculation although none $\delta^{15}N_{NO_3}$ profiles had been published in the southern basin. Future works about $\delta^{15}N_{NO_3}$ and $\delta^{15}N_{SP}$ in the southern AS are needed.

In Fig. 7b, we presented corrected $\delta^{15}N_{bulk}$ values along with bottom depth for northern and southern AS surface sediments for comparison. We can see clearly that after removing site-specific bias caused by bottom depth effect, the values and distribution ranges of $\delta^{15}N_{bulk}$ for both northern and southern AS became smaller and narrower. For the northern AS, the distribution pattern skewed negatively giving a standard deviation of 0.88 ‰, exactly falling in the rage of 7 ~ 9 ‰ for $\delta^{15}N_{NO_3}$ (7 ~ 9 ‰) at the bottom of euphotic zone. As a result, the corrected nitrogen isotopic signals in sediments more truthfully represent the $\delta^{15}N_{NO_3}$ value at the bottom depth of euphotic

BGD
11, 8713–8748, 2014

zone. Meanwhile, the statistically significant difference in $\delta^{15}N_{bulk}$ distribution between northern and southern AS further confirms the feasibility of our classification by using DO isopleth of 25 µmol kg^{-1} at 150 m.

5.3 Bottom-depth effect during different climate stages

In order to better decipher the history of $\delta^{15}N_{NO_3}$ in the bottom euphotic zone of the water column, here in this section, we synthesized almost all available $\delta^{15}N_{bulk}$ of sediment cores reported for the AS (see Fig. 1a for locations). Similar to modern surface sediments, northern and southern groups were defined by the contour line of 25 µmol kg^{-1} DO. The data from core MD-04-2876 is abandoned since the relatively low $\delta^{15}N_{bulk}$ might be influenced by terrigenous inputs (Pichevin et al., 2007). To keep data consistency in temporal scale, we focused on recent 35 ka (Fig. 8a). Unfortunately, data points were less in 0 ~ 6 ka and there were only three sediment cores in southern AS, SK177/11 in this study and NIOP 905 and SO42-74KL in previous studies.

As shown in Fig. 8a, the original $\delta^{15}N_{bulk}$ from the northern (purple dots) and southern AS (green, blue and red curves) are scattering in a wide range from 4.5 to 10.5 ‰ over entire 35 ka. For the southern cores, the temporal variations of $\delta^{15}N_{bulk}$ in core SK177/11 and NIOP 905 (red and blue) had a very similar trend distributing at the lower bound of whole dataset. The mean $\delta^{15}N_{bulk}$ values for SK177/11 and NIOP 905 during glacial period were almost identical, and the deviation in the Holocene was as small as 0.7 ‰. By contrast, the temporal pattern for $\delta^{15}N_{bulk}$ of core SO42-74KL (green) resembles that of NIOP 905 yet with an enrichment in ^{15}N by ~ 2 ‰ throughout entire period. The core SO42-74KL is retrieved from depth of 3212 m, which the deepest among the three cores in southern AS, the positive offset is apparently caused by the bottom depth effect. Thus inference should be made with caution when compare sediment cores from different depths.

Below we take two time spans, 6 ~ 11 ka (Holocene) and 19 ~ 35 ka (glacial), to examine the bottom-depth effect at different climate stages. We ignore transgression pe-

BGD
11, 8713–8748, 2014

riod, which is shorter and more variable in $\delta^{15}N_{bulk}$, to avoid bias caused by dating uncertainties in different studies. Also, we will discuss the peculiar patters for 0 ~ 6 ka later. The mean and standard deviation of reported $\delta^{15}N_{bulk}$ values for the specific time span were plotted against the corresponding depth of the core. Accordingly, we obtained the correction factors for glacial and early Holocene, respectively, for northern and southern AS (Fig. 8b and c). Since only 35 ka was applied in this practice, the long term alteration (Reichart et al., 1998; Altabet et al., 1999) is ignored. The regression curves for modern day (dashed lines) were plotted for comparison.

The difference among regressions of three climate stages in northern AS (Table 2). is not significant (0.41×10^{-3} km^{-1} to 0.60×10^{-3} km^{-1}); however, the regression slopes for northern AS are significantly lower when comparing with that obtained from southern AS throughout all climate status. This might indicates the oxygen content in the northern AS is always lower resulting in a lower degree of alteration. On the other hand, we may not exclude the effect by sedimentation rate change over two stages, thus the oxygen exposure time; unfortunately, insufficient sedimentation rate data in northern AS in previous reports prevents us to implement further analysis.

As for the southern AS, correction factors are always higher than that in northern AS. The overall spatial temporal patterns are in consistent with the oxygen distribution in the Arabian Sea (Olson et al., 1993; Morrison et al., 1999; Pichevin et al., 2007) and agree with the view that DO concentration was the dominant factor for organic matter preservation (Aller, 2001; Zonneveld et al., 2010). Meanwhile, the regression slopes remained high from 0.76×10^{-3} km^{-1} to 1.01×10^{-3} km^{-1} over different climate stages in the southern AS suggesting that environmental situations, thus the correction factor, change less relative to that in the northern AS. For SK177/11, sedimentation rate in Holocene is 2 × higher comparing to that in glacial period; however, the influence caused by sedimentation rate changes is likely not significant enough to alter the regression slopes for the southern AS basing on the small changes in slope (0.93×10^{-3} km^{-1} and 1.01×10^{-3} km^{-1}) .

BGD
11, 8713–8748, 2014

5.4 Insights from temporal changes in geographic $\delta^{15}N_{bulk}$ distribution

Based on the earlier comparison among $\delta^{15}N_{NO_3}$, sinking particles and surface sediments, we recognized the regression intercept is representative of the nitrogen isotope of nitrate source at depth of 100 m. Therefore, the regression-derived intercepts in Table 2 were used to discuss the $\delta^{15}N_{NO_3}$ source at different climate stage, while the slopes were used as correction factors to eliminate the positive shift in $\delta^{15}N_{bulk}$ caused by bottom depth, thus, to get the original signal prior to alteration.

Noticeably, the regression intercepts for both northern and southern AS are higher in the Holocene when compared to that in glacial period indicating the intensified isotopic enrichment in $\delta^{15}N_{NO_3}$ had occurred in entire AS in Holocene and the increment is almost the same to be $\sim$ 1.7 ‰, which is similar to the increase in Eastern Tropical North Pacific but slightly smaller than that in the Eastern Tropical South Pacific (Galbraith et al., 2012). The 120 m sea level increase, which may induce only 0.1 ‰ offset, cannot be the reason for significant increase of average $\delta^{15}N_{bulk}$ in Holocene. Moreover, deviations between northern and southern AS at respective climate stage are almost identical (0.8 ‰ for Holocene and 1.0 ‰ for glacial) indicating a synchronous shift in the relative intensity of denitrification and N_2-fixation over the basin to keep such constant latitudinal gradient of subsurface $\delta^{15}N_{NO_3}$. The pattern of water exchange controls the oxygen supply for intermediate water, thus, the stoichiometry of nutrient source to euphotic zone, resulting in the feedback of nitrogen fixation to denitrification in global scale (Galbraith et al., 2004). Therefore, such a basin wide synchronous increase in $\delta^{15}N_{bulk}$ is likely a global control. The lower intercepts in glacial time (4.3 ‰ for south and 5.3 ‰ for north), which are similar to the global mean $\delta^{15}N_{NO_3}$ in modern day (4.5 $\sim$ 5 ‰, Sigman et al., 1997), illustrates a better ventilation of intermediate water during glacial time in the Arabian Sea (Pichevin et al., 2007). Moreover, the AAIW was prevented from northward at 5° N out of the southern part in modern-AS and even during the late Holocene (You, 1998; Pichevin et al., 2007). A sharp decrease of $\delta^{13}C_{TOC}$ in SK177/11

BGD
11, 8713–8748, 2014

at the start of deglaciation (Fig. 3b) may indicate a rapid change of physical circulation had occurred in characteristics of the intermediate water flowing into the AS.

The intercepts of the northern AS increase continuously from 5.3 to 8.1 from glacial through modern day indicating the relative intensity of denitrification to nitrogen fixation in the northern AS kept strengthening (Altabet, 2007). When we take a close look at the temporal pattern of corrected $\delta^{15}N_{bulk}$ for long cores (Fig. 9), we can see an amplified deviation since 6 ka, during which $\delta^{15}N_{bulk}$ increases continuously in the northern AS yet a totally opposite decreasing trend can be observed for southern AS. The reverse trends indicated that the controlling factors on nitrogen cycle in northern AS deviated from that in the southern AS, which means localized enhancement in specific process had occurred.

Besides the oxygen supply to the intermediate water, the intensity of water column denitrification varies with primary productivity (Altabet, 2006; Naqvi et al., 2006). Strong summer monsoon and winter monsoon drive upwelling or convective mixing to enhance the primary productivity, which in turn intensify denitrification (Altabet et al., 2002; Ganeshram et al., 2002). However, it was reported also that primary productivity did not correlate well with water column denitrification underneath during the Holocene in some parts of northern AS (Banakar et al., 2005 and references therein). Regardless the declining summer monsoon strength since 5500 ka (Hong et al., 2003), the primary productivity in northern AS increases indeed.

Similar to the patterns observed for TOC and TN in this study, indicators for productivity (TOC and Ba/Al ratios) reported by Rao et al. (2010) in the core SK148/4 near SK177/11 increased gradually since the Holocene. Incomplete nitrate consumption can hardly explain the decreasing pattern for all three cores in the southern AS where upwelling intensity is much less relative to that in the north. Moreover, lower TOC/TN ratios observed in Holocene in SK177/11 as mentioned earlier rules out the influence from terrestrial organic input. Therefore, a spatial coupling of denitrification-dependent N_2 fixation is the more plausible cause (Deutsch et al., 2007).

BGD
11, 8713–8748, 2014

We suggested that intensified supply of excess phosphorous (phosphorus in stoichiometric excess of fixed nitrogen) toward the southern AS to stimulate N_2 fixation, subsequently the non-diazotrophs is responsible for the decreasing $\delta^{15}N_{bulk}$ pattern in the southern basin. The intensification in excess phosphorous supply can be driven by enhanced upwelling or intensified subsurface water column denitrification or both. According to the increasing pattern in $\delta^{15}N_{bulk}$ and primary productivity in the northern AS, synergetic processes are suggested. The upwelled water in northern AS basin brings up low N/P water to surface for non-diazotrophs to uptake. If we assume complete consumption, the remaining excess phosphorous after complete consumption will be transported toward south by clockwise surface circulation and advection, therefore, N_2-fixation in the southern AS acts as feedback to balance denitrification changes in the northern AS. This phenomenon is similar to the illustration for the spatial coupling of nitrogen inputs and losses in the Pacific Ocean proposed by Deutsch et al. (2007). Why such forcing to expand the N-S deviation had not occurred before 6 ka warrants more studies.

6 Conclusions

The available data showed that values of $\delta^{15}N_{NO_3}$ at the bottom of euphotic zone ($\sim$ 150 m) were similar to $\delta^{15}N_{SP}$ implying that the source of nutrients for sinking particulate organic matter was largely derived from the depth at around 150 m. Values of sedimentary $\delta^{15}N_{bulk}$ were obviously higher than $\delta^{15}N_{SP}$ in surrounding areas suggesting such shift of sedimentary $\delta^{15}N_{bulk}$ occurred after deposition. It is necessary to remove site-specific bias of $\delta^{15}N_{bulk}$ values caused by bottom depth to retrieve the original signal before alteration. As a result, the corrected nitrogen isotopic signal in sediments could be representative of the value of $\delta^{15}N_{NO_3}$ at the bottom depth of euphotic zone. The bottom-depth effects in the northern AS are various in different climate stages, yet, lower than that in the southern AS in general. The modern surface

BGD
11, 8713–8748, 2014

$\delta^{15}N_{bulk}$ values can be separated statistically into northern and southern AS groups reflecting a special coupling of denitrification to the north and N_2-fixation to the south. This phenomenon is supported by reported N* distribution in modern day. As for historical records, the offset in $\delta^{15}N_{bulk}$ between southern and northern AS remained relatively constant (0.8 ‰ for early Holocene and 1.0 ‰ for glacial) prior to 6 ka indicating a synchronous shift in the relative intensity of denitrification and N_2-fixation over the basin to keep such constant latitudinal gradient of subsurface $\delta^{15}N_{NO_3}$. However, this offset expanded gradually since 6 ka indicating more localized intensifications in denitrification and N_2-fixation had occurred, respectively, in the northern and southern Arabian Seas. The spatial coupling of nitrogen inputs and losses in the Arabian Sea was proposed, yet, the reason why the driving force to expand the N-S deviation had not occurred before 6 ka warrants more studies.

Acknowledgements. This research was supported by the National Natural Science Foundation of China (NSFC 41176059, 91328207). The authors gratefully acknowledge Veeran Yoganandan at Bharathidasan University for the provision of sediment core material.

References

Agnihotri, R., Altabet, M. A., and Herbert, T.: Influence of marine denitrification on atmospheric N_2O variability during the Holocene, Geophys. Res. Lett., 33, L13704, doi:10.1029/2006GL025864, 2006.

Aller, R. C.: Transport and reactions in the bioirrigated zone, in: The Benthic Boundary Layer: Transport Processes and Biogeochemistry, edited by: Boudreau, B. and Jørgensen, B. B., Oxford University Press, Oxford, UK, 269–301, 2001.

Altabet, M.: Variations in nitrogen isotopic composition between sinking and suspended particles: implications for nitrogen cycling and particle transformation in the open ocean, Deep-Sea Res., 35, 535–554, 1988.

Altabet, M.: Isotopic tracers of the marine nitrogen cycle: Present and past, in: Marine organic matter: biomarkers, isotopes and DNA, edited by: Volkman, J. K., Springer-Verlag Berlin Heidelberg, 251–293, 2006.

BGD
11, 8713–8748, 2014

Altabet, M. A.: Constraints on oceanic N balance/imbalance from sedimentary ^{15}N records, Biogeosciences, 4, 75–86, doi:10.5194/bg-4-75-2007, 2007.
Altabet, M. and Francois, R.: Sedimentary nitrogen isotopic ratio as a recorder for surface ocean nitrate utilization, Global Biogeochem. Cy., 8, 103–116, 1994.
Altabet, M., Francois, R., Murray, D. W., and Prell, W. L.: Climate-related variations in denitrification in the Arabian Sea from sediment $^{15}N/^{14}N$ ratios, Nature, 373, 506–509, 1995.
Altabet, M., Murray, D. W., and Prell, W. L.: Climatically linked oscillations in Arabian Sea denitrification over the past 1 my: implications for the marine N cycle, Paleoceanography, 14, 732–743, 1999.
Altabet, M., Higginson, M. J., and Murray, D. W.: The effect of millennial-scale changes in Arabian Sea denitrification on atmospheric CO_2, Nature, 415, 159–162, 2002.
Banakar, V., Oba, T., Chodankar, A., Kuramoto, T., Yamamoto, M., and Minagawa, M.: Monsoon related changes in sea surface productivity and water column denitrification in the Eastern Arabian Sea during the last glacial cycle, Mar. Geol., 219, 99–108, 2005.
Brandes, J. A., Devol, A. H., Yoshinari, T., Jayakumar, D., and Naqvi, S.: Isotopic composition of nitrate in the central Arabian Sea and eastern tropical North Pacific: a tracer for mixing and nitrogen cycles, Limnol. Oceanogr., 43, 1680–1689, 1998.
Brummer, G., Kloosterhuis, H., and Helder, W.: Monsoon-Driven Export Fluxes and Early Diagenesis of Particulate Nitrogen and its $\delta^{15}n$ Across the Somalia Margin, Geological Society, London, Special Publications, 195, 353–370, 2002.
Capone, D. G., Zehr, J. P., Paerl, H. W., Bergman, B., and Carpenter, E. J.: Trichodesmium, a globally significant marine cyanobacterium, Science, 276, 1221–1229, 1997.
Capone, D. G., Subramaniam, A., Montoya, J. P., Voss, M., Humborg, C., Johansen, A. M., Siefert, R. L., and Carpenter, E. J.: An extensive bloom of the N_2-fixing cyanobacterium *Trichodesmium erythraeum* in the central Arabian Sea, Mar. Ecol.-Prog. Ser., 172, 281–292, 1998.
Codispoti, L. and Christensen, J.: Nitrification, denitrification and nitrous oxide cycling in the eastern tropical South Pacific Ocean, Mar. Chem., 16, 277–300, 1985.
Cowie, G. L., Mowbray, S., Lewis, M., Matheson, H., and McKenzie, R.: Carbon and nitrogen elemental and stable isotopic compositions of surficial sediments from the Pakistan margin of the Arabian Sea, Deep-Sea Res. Pt. II, 56, 271–282, 2009.
Deutsch, C., Sarmiento, J. L., Sigman, D. M., Gruber, N., and Dunne, J. P.: Spatial coupling of nitrogen inputs and losses in the ocean, Nature, 445, 163–167, 2007.

BGD
11, 8713–8748, 2014

Falkowski, P. G. and Godfrey, L. V.: Electrons, life and the evolution of Earth's oxygen cycle, Philos. T. R. Soc. B, 363, 2705–2716, 2008.
Galbraith, E. D., Kienast, M., Pedersen, T. F., and Calvert, S. E.: Glacial-interglacial modulation of the marine nitrogen cycle by high-latitude O_2 supply to the global thermocline, Paleoceanography, 19, PA4007, doi:10.1029/2003PA00100, 2004.
Galbraith, E. D., Kienast, M., Albuquerque, A. L., Altabet, M., Batista, F., Bianchi, D., Calvert, S., Quintana, S. C., Crosta, X., Holz, R. D. P., Dubois, N., Etourneau, J., Francois, R., Hsu, T.-C., Ivanochko, T., Jaccard, S., Kao, S.-J., Kiefer, T., Kienast, S., Lehmann, M. F., Martinez, P., McCarthy, M., Meckler, A. N., Mix, A., Möbius, J., Pedersen, T., Pichevin, L., Quan, T. M., Robinson, R. S., Ryabenko, E., Schmittner, A., Schneider, R., Schneider-Mor, A., Shigemitsu, M., Sinclair, D., Somes, C., Studer, A., Tesdal, J. E., Thunell, R., and Yang, J.-Y.: The acceleration of oceanic denitrification during deglacial warming, Nat. Geosci., 5, 151–156, 2012.
Ganeshram, R. S., Pedersen, T. F., Calvert, S. E., and Murray, J. W.: Large changes in oceanic nutrient inventories from glacial to interglacial periods, Nature, 376, 755–758, 1995.
Ganeshram, R. S., Pedersen, T. F., Calvert, S. E., McNeill, G. W., and Fontugne, M. R.: Glacial-interglacial variability in denitrification in the world's oceans: causes and consequences, Paleoceanography, 15, 361–376, 2000.
Ganeshram, R. S., Pedersen, T. F., Calvert, S., and François, R.: Reduced nitrogen fixation in the glacial ocean inferred from changes in marine nitrogen and phosphorus inventories, Nature, 415, 156–159, 2002.
Gaye, B., Wiesner, M., and Lahajnar, N.: Nitrogen sources in the South China Sea, as discerned from stable nitrogen isotopic ratios in rivers, sinking particles, and sediments, Mar. Chem., 114, 72–85, 2009.
Gaye-Haake, B., Lahajnar, N., Emeis, K. C., Unger, D., Rixen, T., Suthhof, A., Ramaswamy, V., Schulz, H., Paropkari, A., and Guptha, M.: Stable nitrogen isotopic ratios of sinking particles and sediments from the northern Indian Ocean, Mar. Chem., 96, 243–255, 2005.
Gouretski, V. and Koltermann, K. P.: WOCE global hydrographic climatology, Berichte des BSH, 35, 1–52, 2004.
Gruber, N.: The dynamics of the marine nitrogen cycle and its influence on atmospheric CO_2 variations, in: The Ocean Carbon Cycle and Climate, edited by: Follows, M. and Oguz, T., Springer Netherlands, 97–148, 2004.
Gruber, N. and Galloway, J. N.: An Earth-system perspective of the global nitrogen cycle, Nature, 451, 293–296, 2008.

BGD
11, 8713–8748, 2014

Gruber, N. and Sarmiento, J. L.: Biogeochemical/physical interactions in elemental cycles, in: The Sea: Biological-Physical Interactions in the Oceans, edited by: Robinson, A. R., McCarthy, J. J., and Rothschild, B. J., John Wiley and Sons, New York, 337–399, 2002.

Haug, G. H., Pedersen, T. F., Sigman, D. M., Calvert, S. E., Nielsen, B., and Peterson, L. C.: Glacial/interglacial variations in production and nitrogen fixation in the Cariaco Basin during the last 580 kyr, Paleoceanography, 13, 427–432, 1998.

Holmes, M. E., Schneider, R. R., Müller, P. J., Segl, M., and Wefer, G.: Reconstruction of past nutrient utilization in the eastern Angola Basin based on sedimentary $^{15}N/^{14}N$ ratios, Paleoceanography, 12, 604–614, 1997.

Hong, Y., Hong, B., Lin, Q., Zhu, Y., Shibata, Y., Hirota, M., Uchida, M., Leng, X., Jiang, H., and Xu, H.: Correlation between Indian Ocean summer monsoon and North Atlantic climate during the Holocene, Earth Planet. Sci. Lett., 211, 371–380, 2003.

Ivanochko, T. S., Ganeshram, R. S., Brummer, G. J. A., Ganssen, G., Jung, S. J. A., Moreton, S. G., and Kroon, D.: Variations in tropical convection as an amplifier of global climate change at the millennial scale, Earth Planet. Sci. Lett., 235, 302–314, 2005.

Kao, S., Lin, F., and Liu, K.: Organic carbon and nitrogen contents and their isotopic compositions in surficial sediments from the East China Sea shelf and the southern Okinawa Trough, Deep-Sea Res. Pt. II, 50, 1203–1217, 2003.

Kao, S., Dai, M., Wei, K., Blair, N., and Lyons, W.: Enhanced supply of fossil organic carbon to the Okinawa Trough since the last deglaciation, Paleoceanography, 23, PA2207, doi:10.1029/2007PA001440, 2008.

Kienast, M., Higginson, M., Mollenhauer, G., Eglinton, T. I., Chen, M. T., and Calvert, S. E.: On the sedimentological origin of down-core variations of bulk sedimentary nitrogen isotope ratios, Paleoceanography, 20, doi:10.1029/2004PA0018081, 2005.

Liu, K.-K. and Kaplan, I. R.: The eastern tropical Pacific as a source of ^{15}N-enriched nitrate in seawater off southern Califomia, Limnol. Oceanogr., 34, 820–830, 1989.

Möbius, J., Gaye, B., Lahajnar, N., Bahlmann, E., and Emeis, K.-C.: Influence of diagenesis on sedimentary $\delta^{15}N$ in the Arabian Sea over the last 130 kyr, Mar. Geol., 284, 127–138, 2011.

Mollenhauer, G., Kienast, M., Lamy, F., Meggers, H., Schneider, R. R., Hayes, J. M., and Eglinton, T. I.: An evaluation of 14C age relationships between co-occurring foraminifera, alkenones, and total organic carbon in continental margin sediments, Paleoceanography, 20, PA1016, doi:10.1029/2004PA001103, 2005.

BGD
11, 8713–8748, 2014

Morrison, J., Codispoti, L., Gaurin, S., Jones, B., Manghnani, V., and Zheng, Z.: Seasonal variation of hydrographic and nutrient fields during the US JGOFS Arabian Sea Process Study, Deep-Sea Res. Pt. II, 45, 2053–2101, 1998.

Morrison, J., Codispoti, L., Smith, S. L., Wishner, K., Flagg, C., Gardner, W. D., Gaurin, S., Naqvi, S., Manghnani, V., and Prosperie, L.: The oxygen minimum zone in the Arabian Sea during 1995, Deep-Sea Res. Pt. II, 46, 1903–1931, 1999.

Nair, R., Ittekkot, V., Manganini, S., Ramaswamy, V., Haake, B., Degens, E., Desai, B. t., and Honjo, S.: Increased particle flux to the deep ocean related to monsoons, Nature, 338, 749–751, 1989.

Naqvi, S.: Denitrification processes in the Arabian Sea, P. Indian AS Earth, 103, 279–300, 1994.

Naqvi, S., Noronha, R. J., and Reddy, C.: Denitrification in the Arabian Sea, Deep-Sea Res., 29, 459–469, 1982.

Naqvi, S. W. A., Naik, H., Pratihary, A., D'Souza, W., Narvekar, P. V., Jayakumar, D. A., Devol, A. H., Yoshinari, T., and Saino, T.: Coastal versus open-ocean denitrification in the Arabian Sea, Biogeosciences, 3, 621–633, doi:10.5194/bg-3-621-2006, 2006.

Olson, D. B., Hitchcock, G. L., Fine, R. A., and Warren, B. A.: Maintenance of the low-oxygen layer in the central Arabian Sea, Deep-Sea Res. Pt. II, 40, 673–685, 1993.

Pandarinath, K., Subrahmanya, K., Yadava, M., and Verma, S.: Late quaternary sedimentation records on the continental slope off southwest coast of India – implications for provenance, depositional and paleomonsoonal conditions, J. Geol. Soc. India, 69, 1285–1292, 2007.

Parab, S. G. and Matondkar, S.: Primary productivity and nitrogen fixation by *Trichodesmium* spp. in the Arabian Sea, J. Marine Syst., 105, 82–95, 2012.

Paulmier, A. and Ruiz-Pino, D.: Oxygen minimum zones (OMZs) in the modern ocean, Prog. Oceanogr., 80, 113–128, 2009.

Pichevin, L., Bard, E., Martinez, P., and Billy, I.: Evidence of ventilation changes in the Arabian Sea during the late Quaternary: implication for denitrification and nitrous oxide emission, Global Biogeochem. Cy., 21, GB4008, doi:10.1029/2006GB002852, 2007.

Rao, V. P., Kessarkar, P. M., Thamban, M., and Patil, S. K.: Paleoclimatic and diagenetic history of the late quaternary sediments in a core from the southeastern Arabian Sea: geochemical and magnetic signals, J. Oceanogr., 66, 133–146, 2010.

BGD
11, 8713–8748, 2014

Reichart, G.-J., Lourens, L., and Zachariasse, W.: Temporal variability in the northern Arabian Sea Oxygen Minimum Zone (OMZ) during the last 225 000 years, Paleoceanography, 13, 607–621, 1998.

Reimer, P. J., Baillie, M. G., Bard, E., Bayliss, A., Beck, J. W., Blackwell, P. G., Ramsey, C. B., Buck, C. E., Burr, G. S., and Edwards, R. L.: IntCal09 and Marine09 radiocarbon age calibration curves, 0–50 000 years cal BP, Radiocarbon, 51, 1111–1150, 2009.

Rixen, T., Haake, B., Ittekkot, V., Guptha, M., Nair, R., and Schlüssel, P.: Coupling between SW monsoon-related surface and deep ocean processes as discerned from continuous particle flux measurements and correlated satellite data, J. Geophys. Res., 101, 28569–28528, 1996.

Robinson, R. S., Brunelle, B. G., and Sigman, D. M.: Revisiting nutrient utilization in the glacial Antarctic: evidence from a new method for diatom-bound N isotopic analysis, Paleoceanography, 19, PA3001, doi:10.1029/2003PA000996, 2004.

Robinson, R. S., Kienast, M., Luiza Albuquerque, A., Altabet, M., Contreras, S., De Pol Holz, R., Dubois, N., Francois, R., Galbraith, E., and Hsu, T. C.: A review of nitrogen isotopic alteration in marine sediments, Paleoceanography, 27, PA4203, doi:10.1029/2012PA002321, 2012.

Schäfer, P. and Ittekkot, V.: Seasonal variability of δ^{15}N in settling particles in the Arabian Sea and its palaeogeochemical significance, Naturwissenschaften, 80, 511–513, 1993.

Schmittner, A., Galbraith, E. D., Hostetler, S. W., Pedersen, T. F., and Zhang, R.: Large fluctuations of dissolved oxygen in the India and Pacific oceans during Dansgaard–Oeschger oscillations caused by variations of North Atlantic Deep Water subduction, Paleoceanography, 22, PA3207, doi:10.1029/2006PA001384, 2007.

Schubert, C. J. and Calvert, S. E.: Nitrogen and carbon isotopic composition of marine and terrestrial organic matter in Arctic Ocean sediments: implications for nutrient utilization and organic matter composition, Deep-Sea Res. Pt. I, 48, 789–810, 2001.

Schulte, S., Rostek, F., Bard, E., Rullkötter, J., and Marchal, O.: Variations of oxygen-minimum and primary productivity recorded in sediments of the Arabian Sea, Earth Planet. Sci. Lett., 173, 205–221, 1999.

Sigman, D., Altabet, M., Michener, R., McCorkle, D., Fry, B., and Holmes, R.: Natural abundance-level measurement of the nitrogen isotopic composition of oceanic nitrate: an adaptation of the ammonia diffusion method, Mar. Chem., 57, 227–242, 1997.

BGD
11, 8713–8748, 2014

Sigman, D., Altabet, M., McCorkle, D., Francois, R., and Fischer, G.: The δ^{15}N of nitrate in the Southern Ocean: nitrogen cycling and circulation in the ocean interior, J. Geophys. Res.-Oceans (1978–2012), 105, 19599–19614, 2000.

Sigman, D. M., Karsh, K. L., and Casciotti, K. L.: Nitrogen isotopes in the ocean, in: Encyclopedia of Ocean Sciences, edited by: John, H. S. (Editor-in-Chief), Academic Press, Oxford, 1884–1894, 2001.

Stuiver, M. and Braziunas, T. F.: Anthropogenic and solar components of hemispheric ^{14}C, Geophys. Res. Lett., 25, 329–332, 1998.

Suthhof, A., Ittekkot, V., and Gaye-Haake, B.: Millennial-scale oscillation of denitrification intensity in the Arabian Sea during the late Quaternary and its potential influence on atmospheric N_2O and global climate, Global Biogeochem. Cy., 15, 637–649, 2001.

Thunell, R. C., Sigman, D. M., Muller-Karger, F., Astor, Y., and Varela, R.: Nitrogen isotope dynamics of the Cariaco Basin, Venezuela, Global Biogeochem. Cy., 18, GB3001, doi:10.1029/2003GB002185, 2004.

You, Y.: Intermediate water circulation and ventilation of the Indian Ocean derived from water-mass contributions, J. Mar. Res., 56, 1029–1067, 1998.

Zonneveld, K. A. F., Versteegh, G. J. M., Kasten, S., Eglinton, T. I., Emeis, K.-C., Huguet, C., Koch, B. P., de Lange, G. J., de Leeuw, J. W., Middelburg, J. J., Mollenhauer, G., Prahl, F. G., Rethemeyer, J., and Wakeham, S. G.: Selective preservation of organic matter in marine environments; processes and impact on the sedimentary record, Biogeosciences, 7, 483–511, doi:10.5194/bg-7-483-2010, 2010.

BGD
11, 8713–8748, 2014

Table 1. AMS ^{14}C dates of sediment core SK177/11. Radiocarbon ages were calibrated using CALIB 6.0 program (http://calib.qub.ac.uk/calib/calib.html, Reimer et al., 2009).

Lab code	Depth cm	Dating materials	pMC	Raw ^{14}C age (yr BP)	Calibrated age (yr BP) (1σ)	δ^{13}C (‰)
KIA24386	58	OM	65.58 ± 0.17	3390 ± 20	3186 ± 24	−18.55 ±0.04
KIA26327	125	OM	46.65 ± 0.20	6125 ± 35	6504 ± 26	−20.02 ±0.10
KIA24387	155	OM	31.38 ± 0.13	9310 ± 30	10054 ± 104	−19.50 ±0.08
KIA26328	175	OM	21.96 ± 0.12	12180 ± 45	13618 ± 104	−17.71 ±0.18
KIA24388	205	OM	13.94 ± 0.11	15830 ± 60	18646 ± 54	−21.65 ±0.15
KIA24389	275	OM	9.81 ± 0.12	18650 + 100(−90)	21774 ± 194	−18.02 ±0.10
KIA26329	355	OM	2.76 ± 0.06	28830 ± 180	32857 ± 207	−19.23 ±0.17

OM-Organic matter; pMC-Percent modern.

BGD
11, 8713–8748, 2014

Table 2. Linear equations of bottom-depth effect during different climate stages.

Location	Northern AS	Southern AS
Modern	$\delta^{15}N = 0.55\,(\pm 0.08) \times 10^{-3} \times \text{Depth} + 8.1\,(\pm 0.2)$ ($R^2 = 0.40$, $n = 78$, $P < 0.0001$)	$\delta^{15}N = 0.76\,(\pm 0.14) \times 10^{-3} \times \text{Depth} + 6.0\,(\pm 0.3)$ ($R^2 = 0.66$, $n = 18$, $P < 0.0001$)
Holocene	$\delta^{15}N = 0.41\,(\pm 0.20) \times 10^{-3} \times \text{Depth} + 6.9\,(\pm 0.3)$ ($R^2 = 0.32$, $n = 15$, $P = 0.0295$)	$\delta^{15}N = 0.93\,(\pm 0.06) \times 10^{-3} \times \text{Depth} + 6.1\,(\pm 0.1)$ ($R^2 = 0.99$, $n = 3$, $P = 0.0420$)
Glacial	$\delta^{15}N = 0.60\,(\pm 0.20) \times 10^{-3} \times \text{Depth} + 5.3\,(\pm 0.3)$ ($R^2 = 0.52$, $n = 15$, $P = 0.0025$)	$\delta^{15}N = 1.01\,(\pm 0.3) \times 10^{-3} \times \text{Depth} + 4.3\,(\pm 0.7)$ ($R^2 = 0.91$, $n = 3$, $^*P = 0.1899$)

* Insignificant by p value.

BGD
11, 8713–8748, 2014

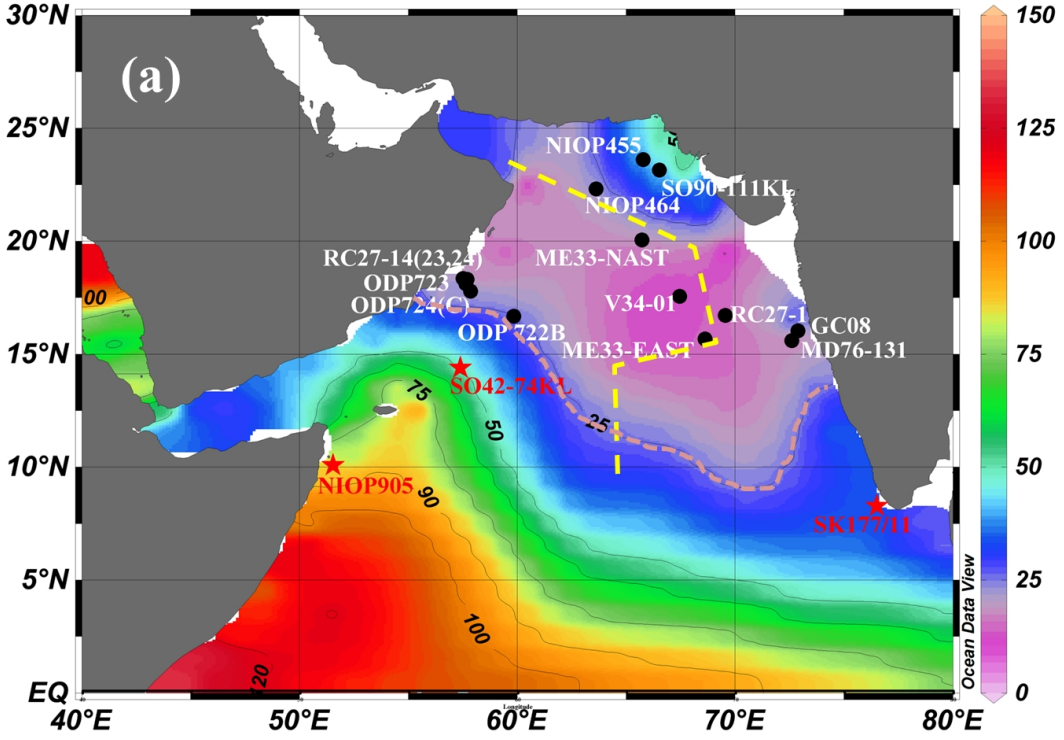

Figure 1. Caption on next page.

BGD
11, 8713–8748, 2014

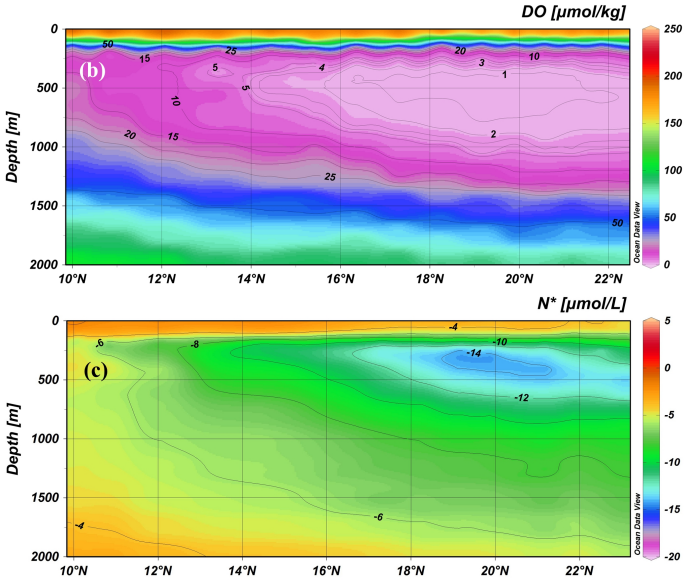

Figure 1. (a) Map of the Arabian Sea. Dissolved oxygen (DO) concentration at 150 m (World Ocean Atlas 09) was shown in color contour. Southern (★) and northern (•) categories of available cores and SK177/11 in this study were defined by DO of 25 µmol kg^{-1} (see text, purple dash curve). **(b)** and **(c)** are DO and N* transects (yellow dashed line in **(a)**, data was originated from data set online of cruises of JGOFS in 1995), respectively, for upper 2000 m. In **(a)**, the northern cores include core NIOP455 vs. NIOP464 (1002 m vs. 1470 m, Reichart et al., 1998), SO90-111KL vs. ME33-NAST (775 m vs. 3170 m, Suthhof et al., 2001), ODP724C vs. ME33-EAST (603 m vs. 3820 m, Möbius et al., 2011), RC27-24 vs. RC27-61 (1416 m vs. 1893 m, Altabet et al., 1995), ODP723 vs. ODP722(B) (808 m vs. 2028 m, Altabet et al., 1999), RC27-14 vs. RC27-23 (596 m vs. 820 m, Altabet et al., 2002), GC08 (2500 m, Banakar et al., 2005); the Southern cores include core SO42-74KL (3212 m, Suthhof et al., 2001), NIOP905 (1586 m, Ivanochko et al., 2005) and SK177/11 (776 m, this study).

BGD
11, 8713–8748, 2014

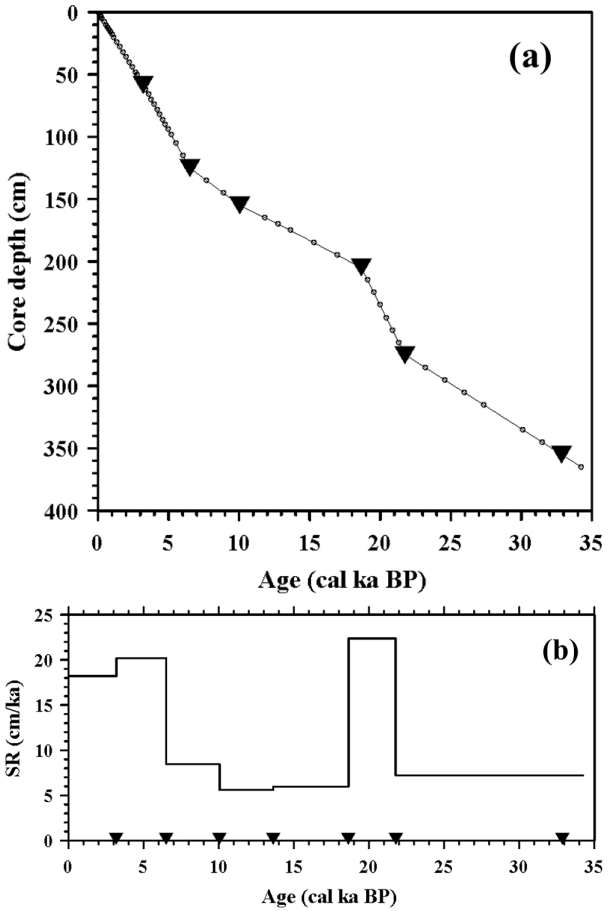

Figure 2. (a) Plot of calendar age against depth; **(b)** Linear sedimentation rate (▼ indicates the ^{14}C age controlling points).

BGD
11, 8713–8748, 2014

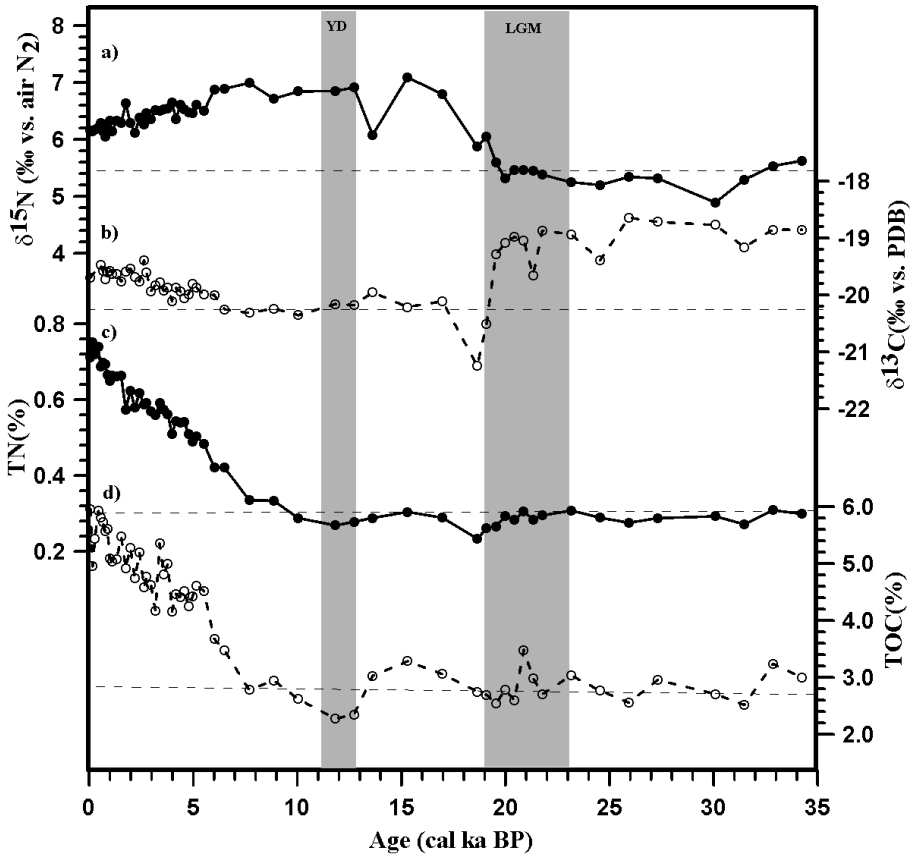

Figure 3. Temporal variations of **(a)** stable isotopic compositions of bulk nitrogen (δ^{15}N), **(b)** stable isotopic compositions of TOC (δ^{13}C), **(c)** contents of total nitrogen and **(d)** total organic carbon. Horizontal dashed lines are references for low value periods.

BGD
11, 8713–8748, 2014

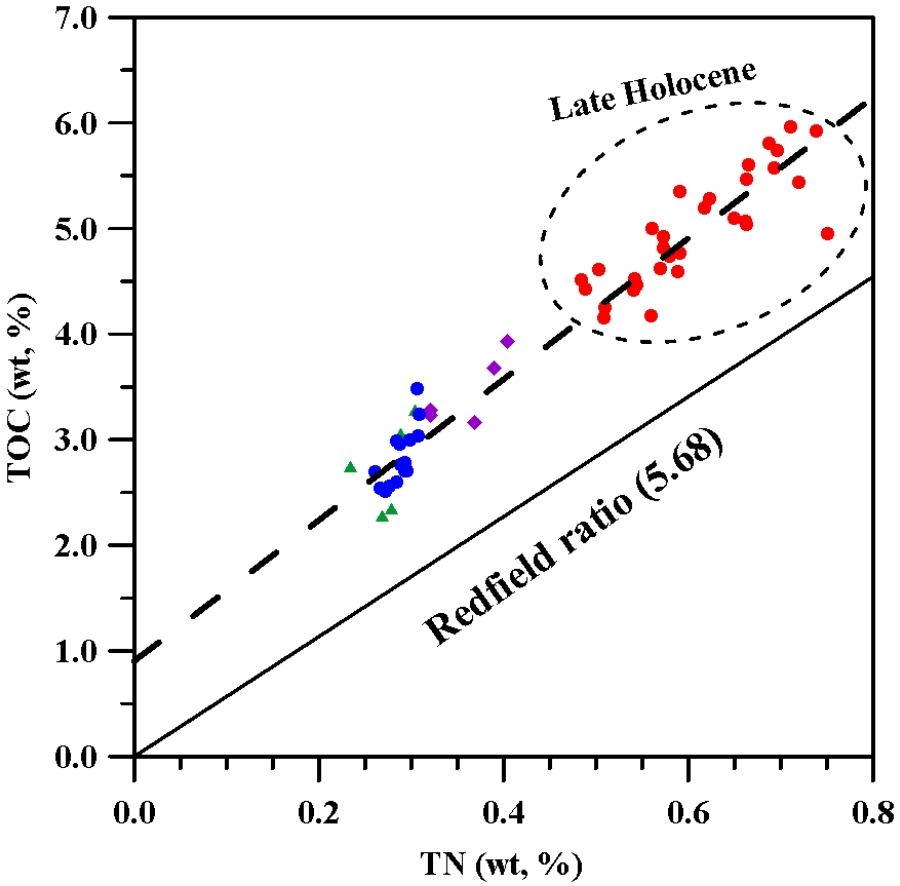

Figure 4. Scatter plot of the total organic carbon content against total nitrogen. Redfield field ratio of 5.68 is shown in line. Dashed line stands for regression. Red, purple, green and blue dots represent the late Holocene, early Holocene, deglacial and glacial periods, respectively.

BGD
11, 8713–8748, 2014

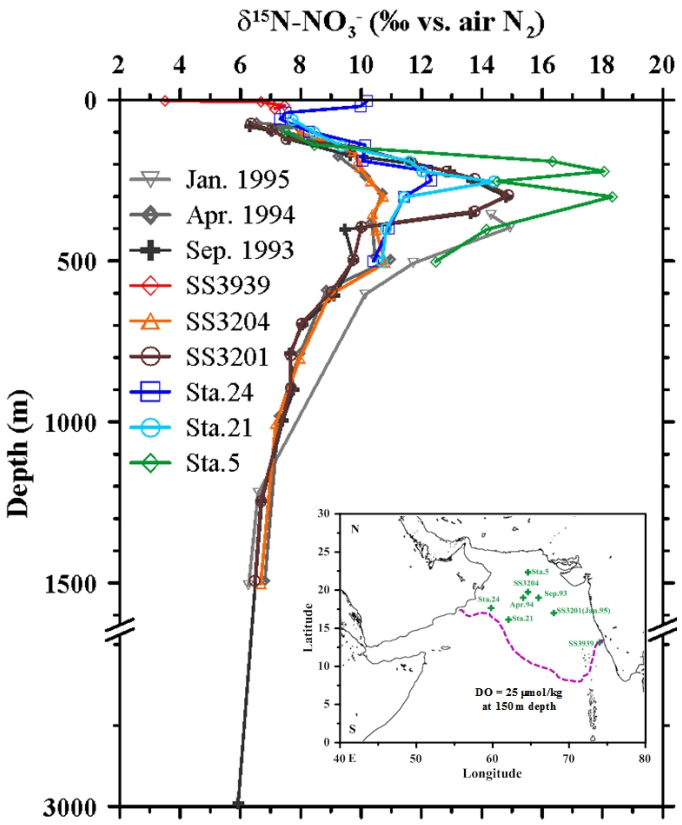

Figure 5. Depth profiles of nitrogen isotope of nitrate ($\delta^{15}N_{NO_3}$) in water column (data without months in mark are all from August and Sta. Jan. 1995 overlaps with Sta. SS3201) (Data digitized from Brandes et al., 1998; Altabet et al., 1999; Naqvi et al., 2006).

BGD
11, 8713–8748, 2014

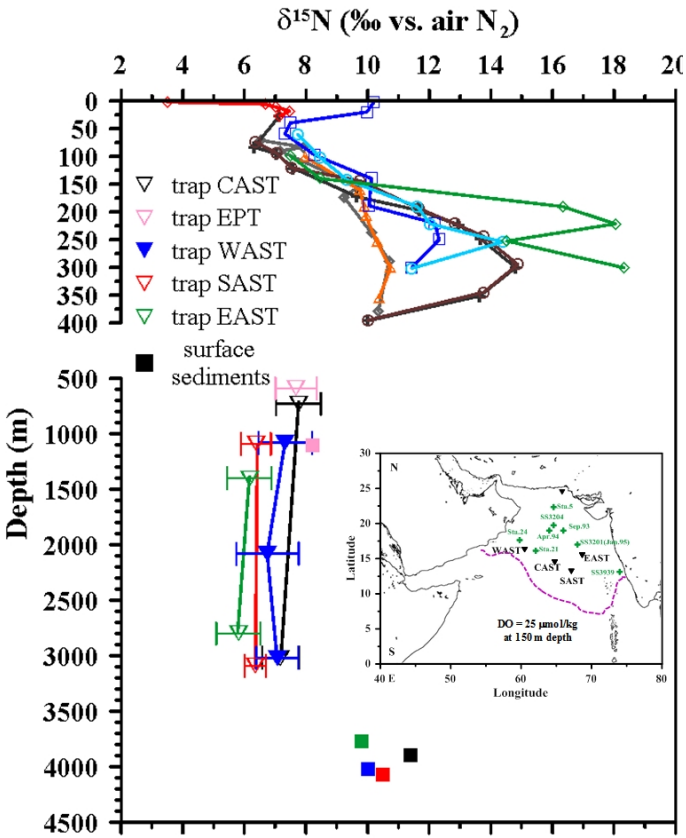

Figure 6. Vertical profiles for nitrogen isotope of nitrate (green crosses in inserted map), sinking particles (inverse triangles in map) and trap-corresponding surface sediments. Data for sediment traps and surface sediments are from Gaye-Haake et al. (2005). Depth profile of $\delta^{15}N_{NO_3}$ follows that in Fig. 5.

BGD
11, 8713–8748, 2014

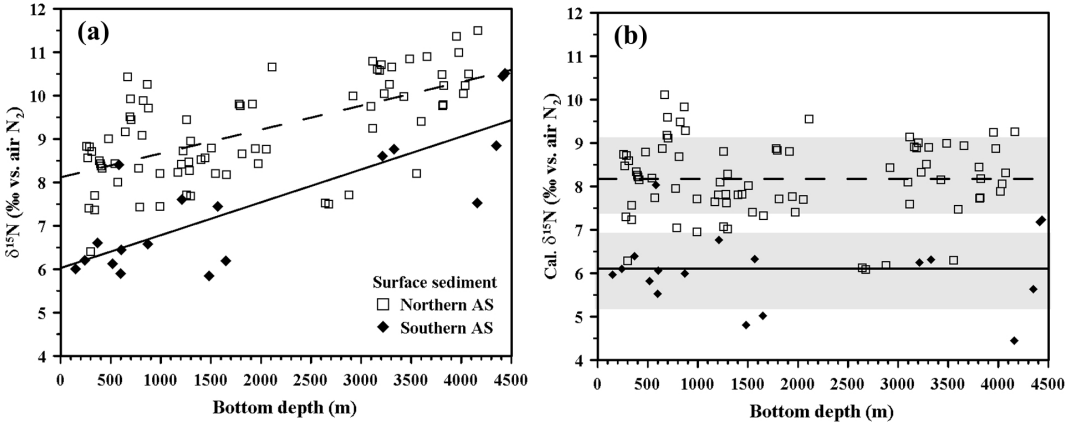

Figure 7. (a) Non-corrected δ^{15}N values of modern surface sediments against corresponding bottom depth in northern and southern Arabian Sea (see text for N–S boundary). Regression lines were shown in dashed and solid lines, respectively, for northern and southern AS. **(b)** Corrected surface sedimentary δ^{15}N values against water depth.

BGD
11, 8713–8748, 2014

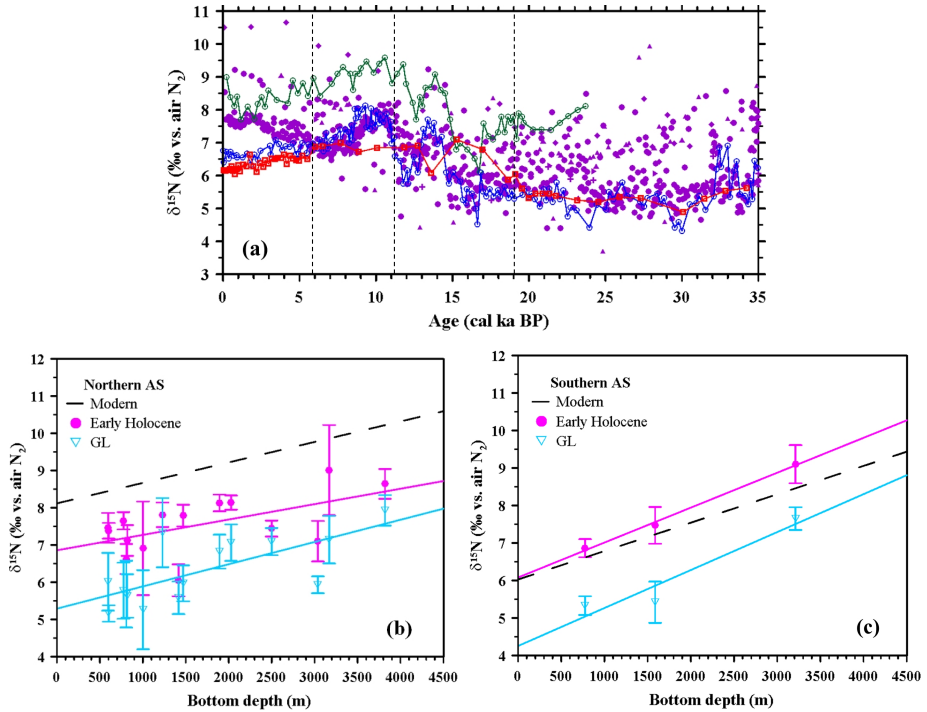

Figure 8. (a) Temporal variations of non-corrected $\delta^{15}N_{bulk}$ values of all reported cores in the AS. Data shown in curves are for cores in the southern Arabian Sea (red for SK177/11, blue for NIOP 905 and green for SO42-74KL), dots in purple are for the northern part. Mean values of $\delta^{15}N$ for fixed periods against corresponding water depths for cores in **(b)** northern and **(c)** southern Arabian Sea. Pink and indigo blue are for Holocene and glacial periods, respectively. Error bars represent the standard deviation for mean $\delta^{15}N_{bulk}$.The dashed regression lines for modern surface sediments are shown for reference.

BGD
11, 8713–8748, 2014

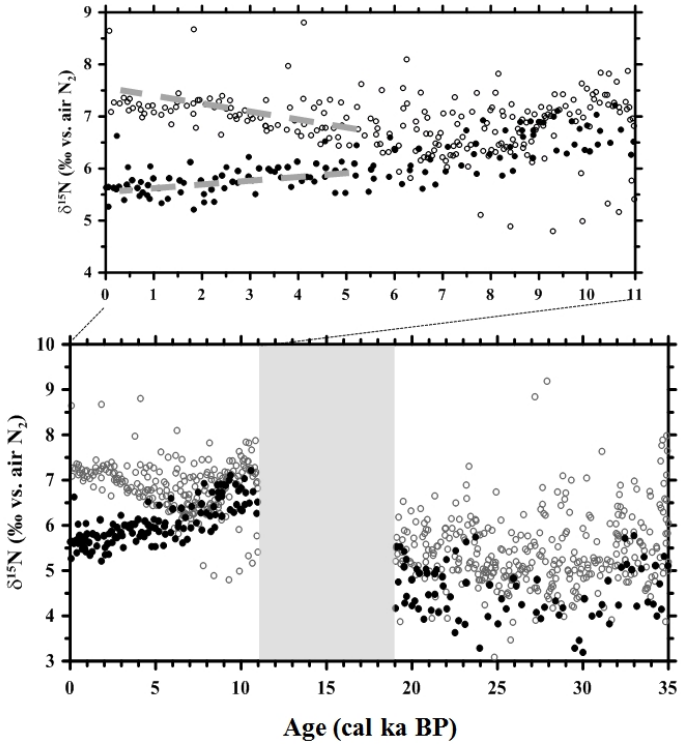

Figure 9. Temporal variations of corrected $\delta^{15}N_{bulk}$ values of all reported cores in the AS. Gray and black dots are for northern and southern AS, respectively. The deglacial period is in shadow because non proper equations for bottom depth effect correction. The upper panel is the blow-up for the Holocene period. The intensified deviation trends since 6 ka were marked by bold dashed lines.

BGD
11, 8713–8748, 2014